Chemical Science

EDGE ARTICLE

View Article Online
View Journal | View Issue

Cite this: *Chem. Sci.*, 2017, **8**, 5662

Macrocycle-assisted synthesis of non-stoichiometric silver(I) halide electrocatalysts for efficient chlorine evolution reaction†

Qiong-You Zhang, ‡ Xin He ‡ and Liang Zhao *

Received 7th February 2017
Accepted 9th June 2017

DOI: 10.1039/c7sc00575j

rsc.li/chemical-science

The electrocatalytic oxidation of chloride to chlorine is a fundamental and important electrochemical reaction in industry. Herein we report the synthesis of non-stoichiometric silver halide nanoparticles through a novel macrocycle-assisted bulk-to-cluster-to-nano transformation. The acquired positively charged nanoparticles expedite chloride transportation by electrostatic attraction and facilitate the formation of silver polychloride catalytic species on the surface, thus functioning as efficient and selective electrocatalysts for the chlorine evolution reaction (CER) at a very low overpotential and within a wide concentration range of chloride. The formation of uncommon non-stoichiometric nanoparticles prevents the formation of a AgCl precipitate and exposes more coordination unsaturated silver atoms to catalyze CER, finally causing a large enhancement of the atomic catalytic efficiency of silver. This study showcases a promising approach to achieve efficient catalysts from a bottom-up design.

Introduction

The chlorine evolution reaction (CER, $2Cl^- \rightarrow Cl_2 + 2e^-$) is one of the most important electrochemical reactions in industry (*e.g.* the chlor-alkali process).[1] The great significance of CER, as reflected by the extensive applications of chlorine in polymers, disinfectants, and drugs *etc.*,[2] has stimulated a tremendous number of studies focused on developing efficient catalysts and an in-depth understanding of related catalytic mechanisms.[3,4] Moreover, CER has also been deemed as a potential alternative to the oxidation of water to oxygen ($2H_2O \rightarrow 4H^+ + O_2 + 4e^-$) in a water-splitting cell because the two-electron CER would consume less energy than the four-electron oxygen evolution reaction (OER). From a thermodynamic viewpoint, OER (equilibrium potential $E^o = 1.23$ V *vs.* NHE) is preferred over CER ($E^o = 1.36$ V).[5] Therefore, in addition to the pursuit of efficient catalysts for making CER proceed at low overpotentials, much effort has also been devoted to achieving high selectivity of the anodic reaction toward CER over OER.[6]

Among the existing classes of electrocatalysts for CER, RuO_2, together with iridium and titanium oxides, constitute the most extensively applicable catalyst family.[7] However, such RuO_2-based anodes tend to be deactivated by surface poisoning[8] and are likely to degrade under harsh conditions (low pH, high current density, *etc.*). Therefore, homogeneous catalysts, such as polypyridine Ru-aqua complexes,[9] Ru-centered coordination polymer derivatives,[10] and ferrocene in micellar media[11] are desirable in order to avoid instability. Although silver(I) has long been recognized as an excellent oxidant and applied in many oxidative coupling reactions,[12] it has been seldom employed as an electrocatalyst for CER due to the easy formation of AgCl precipitate ($K_{sp} = 1.77 \times 10^{-10}$ at 25 °C) and the high potential required for accessing the Ag(II/I) couple ($E^o = 1.98$ V). Recently, Chen and co-workers manifested that the silver(I) polychloride species $[AgCl_2]^-$ and $[AgCl_3]^{2-}$ provided access to the higher formal oxidation states of silver by delocalizing the oxidative charge over the chloride anions and thus catalyzed CER at a low overpotential.[13] However, a high concentration of chloride is required as a prerequisite to avoid AgCl precipitation and to form the catalytic species $[AgCl_n]^{n-1}$ (n = 2–4). Herein, we disclose a facile synthesis of non-stoichiometric silver halide nanoparticles $[Ag_mX_n]^{(m-n)+}$ ($m > n$, X = Cl, Br, I) through a novel macrocycle-assisted bulk-to-cluster-to-nano transformation (Scheme 1). The $[Ag_mX_n]^{(m-n)+}$ nanoparticles can be steadily dispersed in NaCl solution without the formation of AgCl precipitate. The positively charged nature of $[Ag_mX_n]^{(m-n)+}$ expedites chloride transportation by electrostatic attraction and facilitates the formation of a silver polychloride catalytic species on the surface of the nanoparticles, thus functioning as a highly efficient and selective electrocatalyst for CER at a very low overpotential (10 mV) and within a wide concentration range of chloride (0.05–1 M). The non-stoichiometric elemental ratio between the silver and halogen atoms in the newly synthesized

The Key Laboratory of Bioorganic Phosphorus Chemistry & Chemical Biology, Department of Chemistry, Tsinghua University, Beijing 100084, China. E-mail: zhaolchem@mail.tsinghua.edu.cn

† Electronic supplementary information (ESI) available: Supporting figures, high-resolution ESI-MS, TEM images, CV plots and NMR, FT-IR, UV-vis, XPS and AES spectra. Refinement details and crystal data for **1–3** are also available. CCDC 1527294–1527296. For ESI and crystallographic data in CIF or other electronic format see DOI: 10.1039/c7sc00575j

‡ These authors contributed equally.

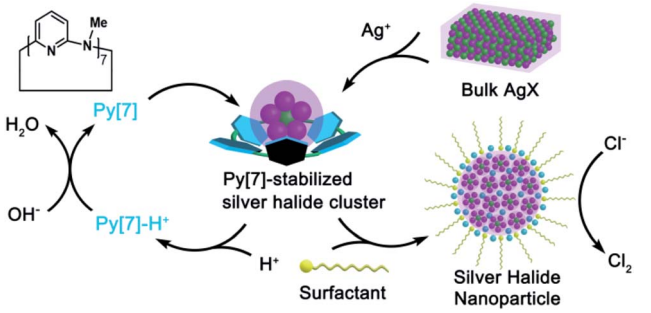

Scheme 1 Macrocycle-assisted bulk-to-cluster-to-nano transformation for the fabrication of non-stoichiometric silver halide nanoparticles as electrocatalysts for CER.

nanoparticles makes the coordination unsaturated silver atoms easily exposed to catalyze the chloride oxidation, consequently resulting in a large enhancement of the atomic catalytic efficiency of silver.

Results and discussion

To date the synthesis of stoichiometric AgX nanoparticles has been extensively reported *via* direct precipitation,[14] reverse micellar/microemulsion,[15] hydrothermal[16] methods, *etc.* It is a formidable challenge to achieve non-stoichiometric silver halide complexes because the stoichiometric compounds AgX are thermodynamically stable. We envisioned that a polydentate macrocyclic ligand would facilitate the formation of a polynuclear silver halide cluster $[Ag_nX]$ ($n > 1$) inside it. The subsequent aggregation of $[Ag_nX]$ would engender the formation of non-stoichiometric silver halide complexes, as shown in Scheme 1. With reference to our previous synthetic methods for silver-sulfide clusters,[17] azacalix[7]pyridine (**Py[7]**) was applied as an outer template to induce the formation of silver halide clusters. Diffusion of diethyl ether into the AgX-$AgCF_3SO_3$-**Py[7]** (X = Cl, Br and I) mixture produced yellow crystals of three silver halide cluster complexes. X-ray crystallographic analysis revealed their formulae as $[Ag_4Cl(CF_3SO_3)_3(\mathbf{Py[7]})(CH_3OH)]$ (**1**), $[Ag_5Br(CF_3SO_3)_2(H_2O)_4(\mathbf{Py[7]})](CF_3SO_3)_2\cdot H_2O$ (**2**) and $[Ag_4I(H_2O)_2(\mathbf{Py[7]})](CF_3SO_3)_3$ (**3**). As shown in Fig. 1, **1**–**3** all comprise a central halide that is encompassed by three or four silver atoms. Each halogen-bonded silver atom is coordinated by one or two pyridyl nitrogen atoms, plus oxygen atoms of triflate groups and solvent molecules, and is further supported by silver–aromatic π interactions (Ag–C distances: 2.515–2.705 Å). The restricted coordination of **Py[7]** gives rise to a systematic variation of the silver–halide bonding from **1** to **3**. In complex **1**, the Ag–Cl bond lengths are in the range of 2.473(3)–2.560(3) Å, approximately 0.2 Å shorter than in reported pyramidal $[Ag_3Cl]$ clusters.[18] Thus, the chlorine atom is 0.34 Å above the Ag1–Ag2–Ag3 plane. In contrast, the long Ag–Br bond lengths of 2.550(2)–2.570(1) Å in **2** cause the bromine atom to be 1.05 Å above the Ag_3 triangle. Due to the small size of the $[Ag_3Cl]$ and $[Ag_3Br]$ clusters, one or two additional silver atoms are included in the **Py[7]** of **1** and **2**. In complex **3**, the Ag–I bond lengths are

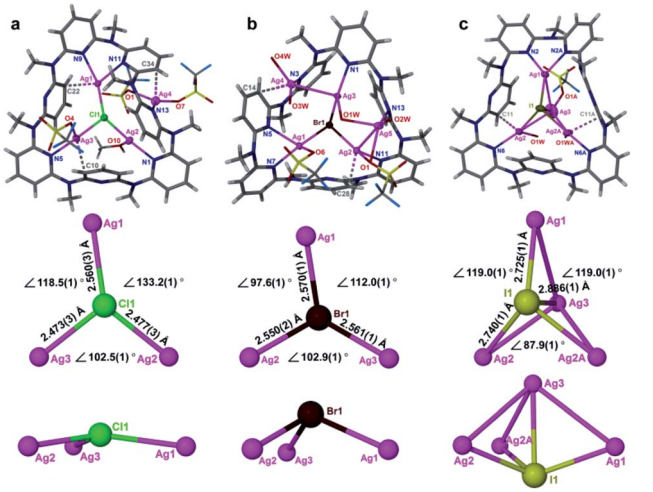

Fig. 1 Crystal structures and silver halide cluster core structures of (a) **1**, (b) **2** and (c) **3**. Some uncoordinated triflates are omitted for clarity. Color coding: Ag, purple; C, black; H, gray; N, blue; O, red; F, cyan; S, yellow; Cl, green; Br, brown; I, dark yellow.

2.725(1)–2.740(1) Å. The expansion of the Ag_3 triangle from **1** to **3** results in the inclusion of one more silver atom capping the silver triangle in **3** through a linkage of Ag–I coordination and threefold argentophilic interactions (2.867(4)–2.909(4) Å).[19] The iodide anion finally bonds to four silver atoms by 0.92 Å above the Ag1–Ag2–Ag2A plane.

The formation of the silver halide clusters $[Ag_{3-4}X]$ inside **Py[7]** in solution was also confirmed by electrospray ionization mass spectrometry (ESI-MS) and elemental analysis (see Fig. S1–S3 in the ESI for details†). The ESI-MS spectrum of **1** displayed two isotopically well-resolved peaks at m/z = 1251.00 and 551.03, corresponding to $[(Ag_3Cl)(\mathbf{Py[7]})(CF_3SO_3)]^+$ and $[(Ag_3Cl)(\mathbf{Py[7]})]^{2+}$, respectively. In addition, the other two observed peaks at m/z = 1506.86 and 678.95 can be ascribed to the above two charged species plus a silver triflate group, respectively (Fig. S1†). Similarly, several $[Ag_3Br]$-related isotopically well-resolved peaks consistent with $[(Ag_3Br)(\mathbf{Py[7]})(CF_3SO_3)]^+$ (m/z = 1295.45), $[(Ag_3Br)(\mathbf{Py[7]})]^{2+}$ (m/z = 573.19), and $[(Ag_3Br)(\mathbf{Py[7]})(CF_3SO_3) + (AgCF_3SO_3)]^+$ (m/z = 1552.39) were observed in the ESI-MS spectrum of complex **2** (Fig. S2†). These ESI-MS experiments confirm the dominant presence of the **Py[7]**-stabilized $[Ag_3Cl]$ and $[Ag_3Br]$ clusters in the solutions of **1** and **2** and the possible involvement of a silver triflate molecule, respectively. The ESI-MS spectrum of the AgI–$AgCF_3SO_3$-**Py[7]** reaction mixture revealed two peaks at m/z = 1342.94 and 595.99, corresponding to the $[(Ag_3I)(\mathbf{Py[7]})(CF_3SO_3)]^+$ and $[(Ag_3I)(\mathbf{Py[7]})]^{2+}$ species, respectively (Fig. S3†). This result is not consistent with the $[Ag_4I]$ cluster, as shown in the crystal structure of **3**, although the composition of complex **3** has been further evidenced by elemental analysis. We hypothesize that the fourth silver atom of the $[Ag_4I]$ cluster may be involved in the crystallization process.

In addition, the biased size matching and unmatching scenarios between **Py[7]** and different silver halide clusters as shown in the crystal structures were also reflected in the ^1H

NMR analysis of **1–3**. In the ^{1}H NMR spectrum of complex **1**, there are two sets of broad peaks at 7.74/7.60 and 6.83/6.72 ppm, corresponding to the pyridyl γ- and β-protons of **Py[7]** (Fig. S4†). The typical downfield shifts relative to the neat **Py[7]** (7.37 and 6.72 ppm for pyridyl γ- and β-protons)[20] suggest the occurrence of coordination between **Py[7]** and silver(I) ions. The broad peaks may result from the many possible conformations of **Py[7]** upon its interaction with the size-unmatching [Ag_3Cl]. In contrast, the ^{1}H NMR spectra of **2** and **3** both exhibit only one set of triplet and doublet sharp signals at 7.77 and 6.85 ppm for the γ- and β-protons of **Py[7]**, respectively (Fig. S5 and S6†). These NMR spectra conflict with the coordination behavior of **Py[7]** in the crystalline structures of **2** and **3**, wherein both coordinated and uncoordinated pyridine rings can be clearly discriminated. In view of the excellent flexibility of azacalixpyridines[20] and the acquired simple proton NMR spectra of **2** and **3**, we conjecture that the conformations of **Py[7]** in **2** and **3** are fluxional at room temperature and the seven pyridyl nitrogen atoms of **Py[7]** undergo a rapid dissociation-recombination equilibrium to bond to the size-matching [Ag_3Br] and [Ag_3I] aggregates relative to the proton NMR time scale.[21]

In contrast to the μ_6-octahedral and μ_4-tetrahedral coordination modes for a halide center in bulk AgX,[22] the above unsaturated μ_3- or μ_4-pyramidal coordination configurations of the halides in **1–3** make free [$Ag_{3-4}X$] clusters prone to aggregation by sharing silver atoms to complete a stable coordination geometry for halogen atoms similar to that in bulk silver monohalides. Tetrafluoroboric acid (HBF_4) was added into the methanol solution of **1** to interrupt the coordination interactions between the central [Ag_3Cl] cluster and the surrounding **Py[7]**. This protonation process led to a colorless-to-yellow color change accompanied by a small amount of white precipitate, which was confirmed as AgCl by powder X-ray diffraction (XRD) analysis (Fig. 2a). Transmission electron microscopy (TEM) photographs taken at different intervals evidenced the formation and stepwise growth of nanometer-sized particles (Fig. S7†). Polyvinylpyrrolidone (PVP) was employed to stabilize the acquired nanoparticles, which were purified by centrifugation and washed with cyclohexane several times to finally produce a sample of **1-NP**. Fourier transform infrared (FT-IR) spectra of **1**, **1-NP**, **Py[7]** and PVP confirmed the successful removal of **Py[7]** and clearly showed the existence of capping PVP in **1-NP** (Fig. S8†). **1-NP** can retain its solution homogeneity in methanol for over one week. Powder X-ray diffraction revealed the poor crystallinity of **1-NP** in comparison with the AgCl sample (Fig. 2a), suggesting a significant difference between **1-NP** and AgCl. TEM images of **1-NP** revealed a dispersion diameter of 2.5 ± 1.5 nm (Fig. 2b). Similar synthetic procedures were applied to produce PVP-stabilized silver bromide (**2-NP** in 2.0 ± 1.5 nm) and silver iodide (**3-NP** in 2.5 ± 1.0 nm) nanoparticles (Fig. 2c and d). Notably, the acidified **Py[7]** ligands can be recycled after neutralization and extraction.

We next investigated the oxidation state of silver in **1-** to **3-NP** by comparing their absorption spectra with those of previously reported $Ag^{(I)}X/Ag^{(0)}$ mixed valence nanoparticles.[14,23] As shown in Fig. S9,† the absorption spectra of the methanol solutions of

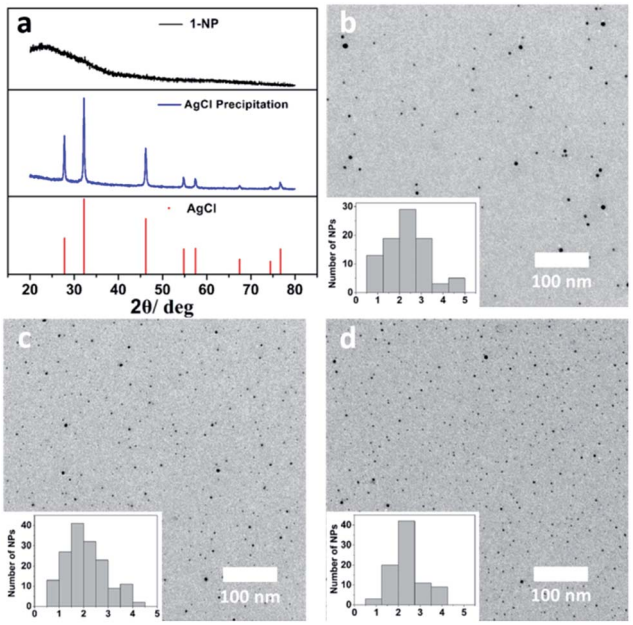

Fig. 2 (a) XRD patterns of the acquired white AgCl precipitate, **1-NP** and reference AgCl (JCPDS file: 31-1238). TEM images and size-distribution histograms of (b) **1-NP**, (c) **2-NP**, and (d) **3-NP**.

1- to **3-NP** exhibited a monotonic decrease in the whole recorded range of 200–1000 nm, plus several shoulder peaks. For example, **1-NP** showed strong absorption with three shoulder peaks at 264, 321 and 380 nm in the ultraviolet spectral region (<400 nm) and weak absorption in the visible region, which is similar to the absorption spectrum of a reported PVP-stabilized AgCl nanoparticle sample.[14] **2-NP** and **3-NP** displayed similar monotonic decreases in their absorption spectra, with two shoulder peaks at 260/300 nm and 260/425 nm, respectively. The shoulder peaks in **1-** to **3-NP** may be ascribed to the transition from $4d^{10}$ to $4d^95s^1$ for silver(I) and the surface plasmon resonance (SPR) of silver(I) halide nanoparticles in different sizes, as reported in the literature.[24] The acquired absorption spectra of **1-** to **3-NP** are in sharp contrast to the UV-vis spectra of the $Ag^{(I)}X/Ag^{(0)}$ mixed valence nanoparticles, which exhibit strong absorption in the visible and near-infrared regions due to the strong SPR coupling of the adjacent Ag nanograins or nanoshells.[25] The result of this comparison is evidence that there is no reduction of Ag(I) to Ag(0) in the formation process of silver halide nanoparticles **1–3-NP**.

X-ray photoelectron spectroscopy (XPS) and Auger electron spectroscopy (AES) were then conducted to confirm the 1+ oxidation state of the silver in **1–3-NP** (Fig. 3). Based on the AES data (1130.9 eV) under X-ray irradiation of 1486.7 eV and the XPS data (368.1 eV for Ag $3d^{5/2}$) (Fig. 3a), the Auger parameter of **1-NP** was deduced to be 723.9 eV, which is in good agreement with the standard silver(I) sample, $AgCF_3CO_2$ (Auger parameter: 723.9 eV).[26] The presence of Ag(I) in **2-NP** and **3-NP** was supported by XPS and AES studies as well (Fig. 3b and c), according to the calculated Auger parameters of 723.3 and 724.3 eV, respectively. In consideration of the lack of oxidation state change for silver in the nanoparticle formation process, as

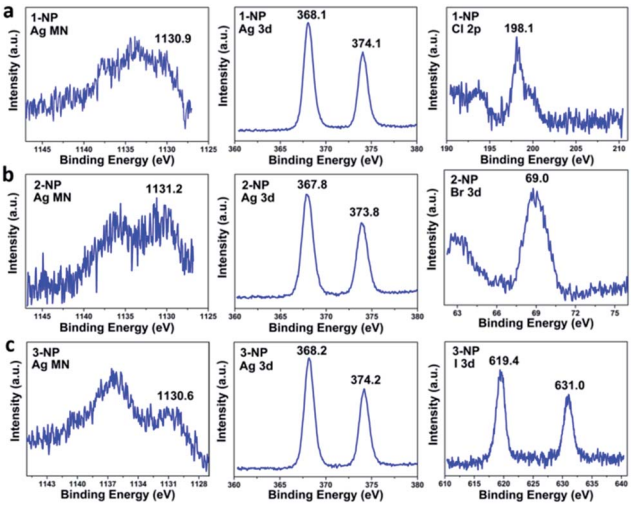

Fig. 3 (a) Ag MN, Ag 3d and Cl 2p signals for **1-NP**. (b) Ag MN, Ag 3d and Br 3d signals for **2-NP**. (c) Ag MN, Ag 3d and I 3d signals for **3-NP**. The Ag MN signals were determined by AES, while the binding energies for Ag 3d, Cl 2p, Br 3d and I 3d were measured by XPS.

shown in eqn (1), the coalescence and fusion of the silver(I)-rich clusters [$Ag_{3-4}X$], accompanied by the formation of the AgX precipitate, should engender the formation of silver halide nanoparticles with a Ag/X elemental ratio higher than 1 : 1 in theory. XPS studies on the elemental content of **1-NP** indeed revealed the Ag/Cl molar ratio as 7.7 : 1 (Fig. 3a). We further measured the energy dispersive X-ray spectrum (EDX) of **1-NP**, which further confirmed the dominant presence of the Ag element over Cl and finally gave the Ag/Cl atomic ratio as 4.6 (Fig. S10†). The Ag/X ratios in **2-NP** and **3-NP** were determined to be 4.7 : 1 and 6.5 : 1, respectively, based on the XPS measurements (Fig. 3b and c). Further taking into account the charge balance, we conjecture that the non-stoichiometric silver halide nanoparticles are positively charged and their outer surface may be surrounded by anions (*e.g.* $CF_3SO_3^-$ and/or BF_4^-). This structural model was then substantiated by Zeta potential measurements, which gave a negative value of −16.0 mV for **1-NP** in aqueous solution.

$$Ag_mX + Ag_mX \rightarrow AgX + Ag_{(2m-1)}X \quad (1)$$

We next investigated the electrochemical oxidation of chloride to chlorine with **1–3-NP** as catalysts. Cyclic voltammetry (CV) measurements were carried out using a glassy carbon (GC) electrode (0.071 cm^2) in an aqueous solution of NaCl (1 M) and HNO_3 (pH ∼ 1, 0.1 M) according to the literature method.[13] As shown in Fig. 4a, the addition of **1-NP** (c_{Ag^+} = 5.3 μM based on inductively coupled plasma/optical emission spectrometry (ICP/OES)) largely enhanced the catalytic current density to 8.36 mA cm^{-2} with E_{onset} = 1.37 V. This E_{onset} value is only 10 mV larger than $E^o(Cl^-/Cl_2)$ = 1.36 V but is remarkably lower than $E^o(Ag^{II/I})$ = 1.98 V. The observation of a typical Cl_2-to-Cl^- reductive wave at around 0.96 V confirmed the occurrence of CER.[9,13] When **2-NP** (c_{Ag^+} = 5.0 μM) and **3-NP** (c_{Ag^+} = 6.7 μM) are employed, E_{onset} is

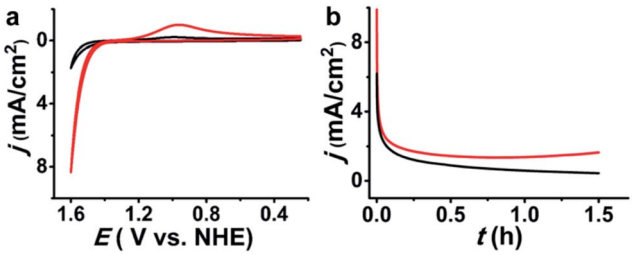

Fig. 4 (a) CVs of a GC electrode in an aqueous solution of NaCl (1 M) and HNO_3 (pH ∼ 1, 0.1 M) without (black) and with (red) **1-NP** (c_{Ag^+} = 5.30 μM). Scan rate: 100 mV s^{-1}. (b) Controlled potential electrolysis curves of **1-NP** at 20 °C (black) and 40 °C (red).

1.37 V as well and the catalytic current density can reach 8.54 and 9.32 mA cm^{-2}, respectively (Fig. S11†). In contrast, a 10-fold higher concentration of silver (c_{Ag^+} = 50 μM) is required to achieve a similar catalytic current density of 8.5 mA cm^{-2} in the reported silver polychloride-catalyzed CER.[13] **1-NP** as a representative example is investigated in detail below.

The scope of the silver halide nanoparticle catalyzed CER was subsequently investigated for practical application. Within a wide concentration range of NaCl from 0.05 to 1 M, typical CV curves for CER with apparent catalytic currents were observed with a low loading of **1-NP** (c_{Ag^+} = 0.56 μM). The linear relationship between the catalytic current density and the NaCl concentration/the loading of catalyst (Fig. S12†) suggests that the catalyst **1-NP** can maintain its structure without forming larger nanoparticles or an insoluble AgCl precipitate, and can keep its catalytic ability in different concentrations of NaCl. On the other hand, the high similarity of the UV-vis absorption spectra of **1-NP** in NaCl solution and in aqueous solution also suggests that no nanoparticle agglomeration takes place (Fig. S13†). In addition, **1-NP** performed very well for the catalytic CER in neutral solution. In a NaH_2PO_4/Na_2HPO_4 aqueous buffer (0.1 M, pH ∼ 7 based on acidometer) of NaCl (c = 0.55 M just as sea water), a low loading of **1-NP** (c_{Ag^+} = 0.53 μM) produced an apparent catalytic current with E_{onset} slightly shifted to 1.31 V (Fig. S14†). The diminishment of the Cl_2-to-Cl^- reductive wave during the reverse scan can be ascribed to the disproportionation of Cl_2 to $HClO/ClO^-$, as reported in a previous study.[27]

Controlled potential electrolysis experiments were performed to evaluate the catalytic efficiency of **1-NP**. Using a large GC plate electrode (1.0 cm^2) at 1.6 V in a solution of NaCl (1 M), HNO_3 (0.1 M, pH ∼ 1) and **1-NP** (c_{Ag^+} = 5.3 μM), the electrocatalytic current was monotonically decreased and finally sustained at a stable current density level of ∼0.7 mA cm^{-2} (Fig. 4b). Cl_2 was swept from the reaction solution by a slow purging N_2 flow into a KI/starch aqueous solution to determine the amount of Cl_2 by iodometric titration. The production of 24.4 μmol of Cl_2 over an electrolysis period of 1.5 h gave a faradaic efficiency of 75%, which is comparable with previous electrocatalysts.[9–11,13] In addition, we found that the stable current density in the electrolysis was temperature dependent. At 40 °C the current density was sustained at ∼1.8 mA cm^{-2}

(Fig. 4b). This result suggests a relationship between the catalytic efficiency and the transportation of chloride.

During and after the electrocatalytic reaction of **1-NP**, we did not find any insoluble solid or suspension in the reaction vial in concentrated or diluted (low to 0.025 M) NaCl solution. Generally, we should observe the formation of silver chloride precipitate due to the aggregation of unprotected nanoparticles if the PVP ligands are totally replaced by chloride. Therefore, we believe that the catalytic species is still PVP-protected. After the controlled potential electrolysis, we measured the CV of the electrolyte solution, which is almost identical to the CV curve measured before the electrolysis (Fig. S15†). This result confirmed the good stability of the catalytic species.

To gain further insight into the possible mechanism accounting for the high catalytic efficiency of **1-NP**, we conducted several contrast experiments. We found that **1-NP** turned into smaller particles with a size dispersion of 1.6 ± 0.7 nm (Fig. 5a) upon being added into a concentrated aqueous solution of NaCl (1 M). In contrast, if the concentration of NaCl is as low as 0.05 M, there is no apparent size change for **1-NP** (Fig. S16†). Such a size change was also observed in the 1 M NaCl solutions of **2-NP** and **3-NP**, which finally gave a size dispersion of 1.5 ± 0.9 and 1.4 ± 0.7 nm, respectively (Fig. S16†). In view of the proposed structural model for **1-NP** that comprises a $[Ag_mCl_n]^{(m-n)+}$ ($m > n$) core surrounded by PVP and anionic BF_4^- and $CF_3SO_3^-$, such a size change may arise from fragmentation of the core by using the strong Ag–Cl coordination in place of the weak coordination between Ag(I) and BF_4^-/$CF_3SO_3^-$. We assumed that smaller nanoparticles may possess a larger surface area and may expose more silver atoms to chloride, thus enhancing the atomic catalytic efficiency of silver. This conjecture was subsequently evidenced by catalytic reaction studies of larger sized **1-NP** (6.0 ± 3.0 nm). This large sample was intentionally synthesized by prolonging the growth time of the nanoparticles from 2 minutes to 10 minutes. CV measurement using the large sample of **1-NP** as the electrocatalyst showed a 40% decrease in the catalytic current density (4.96 mA cm^{-2}) relative to the small sample of 2.5 ± 1.5 nm (8.36 mA cm^{-2}) (Fig. S17†).

The attachment of Cl^- onto **1-NP** was further substantiated by EDX monitoring. Upon adding **1-NP** in the 1 M NaCl solution, we observed an increase of the Ag/Cl ratio from 4.6 : 1 to 1.1 : 1 in EDX studies (Fig. S18†). Meanwhile, the XRD pattern of a **1-NP** sample in 1 M NaCl revealed the appearance of weak peaks corresponding to crystalline AgCl (Fig. S19†). However, after controlled potential electrolysis for 1 h, the Ag/Cl ratio in the EDX measurement changed back to 3.7 : 1 (Fig. S20†). These results indicate an unusual recycling of the Ag/Cl ratio in the catalytic process, which is in good agreement with the proposed catalytic mechanism, *vide infra*.

Moreover, at a low concentration of 0.1 M NaCl the catalytic current density experienced linear growth along with the increase of catalyst loading at the first stage, which is similar to the trend in 1 M NaCl solution. However, the catalytic current gradually approached a saturated value of 1.4 mA cm^{-2} with c_{Ag+} above 1 M, suggesting a possible correlation between the catalytic current density and chloride transportation (Fig. 5b). We assumed that the positive $[Ag_mCl_n]^{(m-n)+}$ ($m > n$) cores may facilitate the transportation of chloride by electrostatic attraction. This assumption was evidenced by a comparison with PVP-stabilized stoichiometric AgCl nanoparticles (**AgCl-NP**).[14] The Ag/Cl ratio of **AgCl-NP** was determined as 0.8 based on XPS studies (Fig. S21†). In contrast to the catalytic current density of 8.36 mA cm^{-2} for the **1-NP**-catalyzed CER (c_{Ag+} = 5.30 μM), a comparable catalyst loading (c_{Ag+} = 4.89 μM based on ICP/OES) of **AgCl-NP** gave a low current density of 3.80 mA cm^{-2} (Fig. 5c). Further increasing the loading of **AgCl-NP** engendered the formation of the precipitate and caused a sharp decrease of the catalytic current. In addition, we evaluated the catalytic selectivity of CER over OER in the **1-NP**-catalyzed system based on the detection of the reduction peaks for Cl_2 and O_2 in the CV study. As shown in Fig. 5d, when the electrolyte solution (c_{NaCl} = 1 M, c_{HNO3} = 0.1 M, pH ∼ 1) was subjected to degassing treatment, the acquired CV curve only showed a Cl_2-to-Cl^- reductive wave at 0.94 V over twenty cycles. In contrast, upon injecting oxygen gas into the system a reductive wave at 0.26 V was observed promptly, which can be assigned as the reductive wave of oxygen. Such high selectivity for CER over OER in the **1-NP**-catalyzed reaction can be ascribed to the fact that the positive $[Ag_mCl_n]^{(m-n)+}$ ($m > n$) core can attract and bond to anionic chlorides more easily than neutral water molecules.

Combining all of the above experimental results, we propose a catalytic mechanism for the **1–3-NP**-catalyzed CER (Scheme 2). By using the macrocycle-assisted bulk-to-cluster transformation, the Ag/X ratio in the resulting macrocycle-encircled silver halide clusters is fixed at three or four. The aggregation of the $[Ag_{3-4}X]$ clusters would generate a number of Ag_mX_n ($m >$

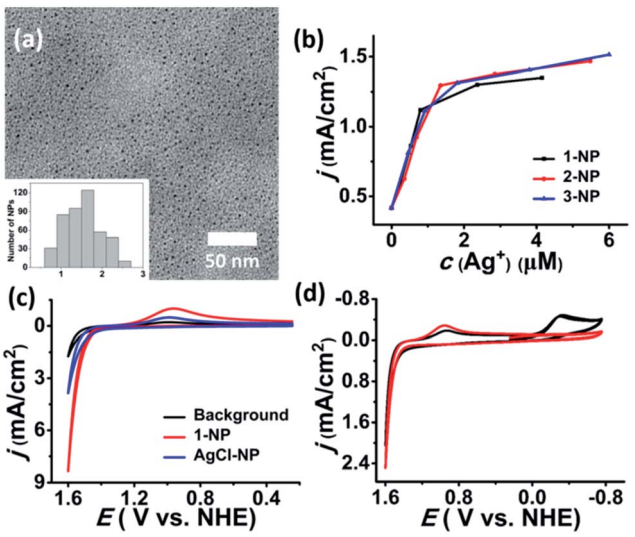

Fig. 5 (a) TEM image of **1-NP** in an aqueous solution of 1 M NaCl. (b) Plot of catalytic current density *vs.* the silver(I) concentrations of **1–3-NP** (0.1 M NaCl, 0.1 M HNO_3). (c) CVs of a GC electrode in an aqueous solution of NaCl (1 M) and HNO_3 (pH ∼ 1, 0.1 M) without (black) and with (red) **1-NP** (c_{Ag+} = 5.30 μM) and with (blue) **AgCl-NP** (c_{Ag+} = 4.89 μM). (d) CVs of a GC electrode in an aqueous solution of NaCl and HNO_3 with **1-NP** (c_{Ag+} = 0.53 μM) as a catalyst after degassing (red) or after bubbling oxygen (black). Scan rate: 100 mV s^{-1}.

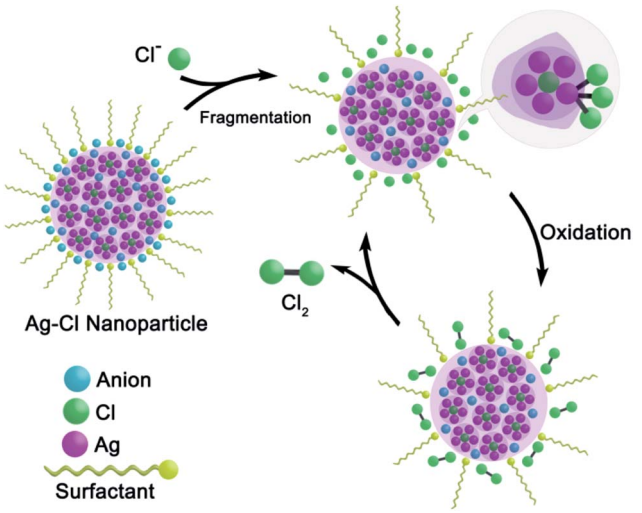

Scheme 2 Proposed mechanism for the catalytic oxidation of chloride to chlorine by non-stoichiometric silver chloride nanoparticles **1-NP**.

n, X = Cl, Br and I) particles at first. These silver halide particles assemble into large nanoparticles, **1–3-NP**, with the assistance of anionic BF_4^- and $CF_3SO_3^-$. **1–3-NP**s are peripherally surrounded by stabilizing PVP and anionic BF_4^- and $CF_3SO_3^-$ for charge balance. The addition of **1–3-NP** into an aqueous solution of NaCl results in the fragmentation of large nanoparticles into small ones due to strong Ag–Cl bonding. The surface silver(I) atoms of $[Ag_mX_n]^{(m-n)+}$ prefer to be coordinated by several chloride ligands for the sake of charge balance and the resulting silver polychloride species make CER take place at a low overpotential by delocalizing the oxidative charge over the chloride anions. In the final step, neutral Cl_2 molecules are drained away and the Ag/X ratio changes back to be larger than 1 : 1. The resulting positive nanoparticle catalysts make the catalytic CER reaction recycle and proceed. However, since the amorphous non-stoichiometric silver halide nanoparticles **1-** to **3-NP** are still structurally unknown, the present proposed catalytic mechanism needs to be further substantiated in the future.

Conclusions

In summary, we have described the first synthesis of a series of PVP-stabilized non-stoichiometric silver halide nanoparticles by virtue of a macrocycle-assisted bulk-to-cluster-to-nanoparticle transformation process. These non-stoichiometric silver halide nanoparticles have a special Ag/X ratio larger than 1 : 1 and exhibit high efficiency and good selectivity in the catalytic oxidation of chloride to chlorine at a low overpotential and within a wide range of chloride concentrations. Mechanistic studies correlate their excellent catalytic performance with the positively charged nature and unsaturated coordination of the $[Ag_mX_n]^{(m-n)+}$ ($m > n$, X = Cl, Br and I) cores. This study showcases a promising approach to achieve highly efficient catalysts from a bottom-up design. We foresee the preparation of many other non-stoichiometric binary catalysts applicable for catalytic reactions by the synthetic protocol reported in this work.

Experimental

Materials and methods

All commercially available chemicals were used without further purification. Heptmethylazacalix[7]pyridine (**Py[7]**) was synthesized according to a literature method by a [3 + 4] fragment coupling protocol between a terminal dibrominated linear trimer and a terminal diaminated linear tetramer.[20] The solvents used in this study were processed by standard procedures. ^{1}H NMR experiments were carried out on a JEOL ECX-400 MHz instrument. The morphology and size distribution of the as-prepared **1-** to **3-NP** nanoparticles were determined with a Hitachi H-7650 transmission electron microscope. X-ray photoelectron spectroscopy was performed on a Thermo Scientific ESCALab 250Xi using 200 W monochromated Al Kα radiation. The 500 μm X-ray spot was used for XPS analysis. The base pressure in the analysis chamber was about 3×10^{-10} mbar. Typically the hydrocarbon C 1s line at 284.8 eV from the adventitious carbon was used for energy referencing.

General synthesis of complexes 1–3

To a CH_3OH (1 mL) suspension of $AgSO_3CF_3$ (38.6 mg, 0.15 mmol) and AgX (0.05 mmol, 7.2 mg for AgCl, 9.5 mg for AgBr and 11.8 mg for AgI), a CH_2Cl_2 solution (1 mL) of **Py[7]** (7.4 mg, 0.01 mmol) was added dropwise. The mixture was further stirred for 5 hours at room temperature and filtered. The filtrate was diffused by diethyl ether in the dark to obtain crystals of complexes **1–3**. Complex **1**: pale yellow needle-like crystals, 13.0 mg, yield 75% based on **Py[7]**. Elemental analysis for $[Ag_4Cl(CF_3SO_3)_3(\mathbf{Py[7]})(CH_3OH)]\cdot(H_2O)_2$ (**1** + $(H_2O)_2$, $C_{46}H_{50}Ag_4ClF_9N_{14}O_{12}S_3$), found (calcd): C, 31.71 (32.03); H, 2.71 (2.92); N, 11.45 (11.37). Complex **2**: pale yellow needle-like crystals, 13.0 mg, yield 65% based on **Py[7]**. Elemental analysis for $[Ag_5Br(\mathbf{Py[7]})](CF_3SO_3)_4\cdot(H_2O)_2$ (**2**–$(H_2O)_3$, $C_{46}H_{46}Ag_5BrF_{12}N_{14}O_{14}S_4$), found (calcd): C, 28.00 (27.70); H, 2.49 (2.32); N, 9.72 (9.83). Complex **3**: pale yellow needle-like crystals, 10.0 mg, yield 56% based on **Py[7]**. Elemental analysis for $[Ag_4I(H_2O)_2(\mathbf{Py[7]})](CF_3SO_3)_3$ (**3**, $C_{45}H_{46}Ag_4IF_9N_{14}O_{11}S_3$), found (calcd): C, 30.43 (30.29); H, 2.68 (2.60); N, 10.78 (10.99).

Synthesis of 1–3-NP. *In situ* deprotection of **Py[7]** was conducted by adding HBF_4 (0.05 mmol) into a methanol/dichloromethane (v/v = 5 : 1) mixed solution (3 mL) of silver halide clusters **1–3** (0.01 mmol). Two minutes later, a methanol (2 mL) solution of poly(vinylpyrrolidone) (PVP, 80 mg, MW ~ 40 000) was then added. The solution was transferred to a centrifuge tube, followed by centrifugation at 10 000 rpm for 10 min. The top solution was removed carefully by a pipette, while the bottom solid product was washed three times with cyclohexane. The solids of **1-** to **3-NP** were dispersed in methanol or de-ionized water for characterization and catalytic studies.

X-ray crystallography

Single-crystal X-ray data for complexes **1–3** were collected at 173 K with Mo-Kα radiation (λ = 0.71073 Å) on a Rigaku Saturn 724/724 + CCD diffractometer with frames of oscillation range 0.5°. The selected crystal was mounted onto a nylon loop by polyisobutene and enveloped in a low-temperature (173 K) stream of

dry nitrogen gas during data collection. The absorption corrections were applied using multi-scan methods. All structures were solved by direct methods, and non-hydrogen atoms were located from difference Fourier maps. Non-hydrogen atoms were subjected to anisotropic refinement by full-matrix least-squares on F^2 using the SHELXTL program[28] unless otherwise noted. The CCDC numbers for the reported complexes are 1527294 (**1**), 1527295 (**2**) and 1527296 (**3**).† The refinement details and crystal data for **1–3** are summarized in the ESI.†

Electrochemical measurements

Electrochemical measurements were performed on an electrochemical workstation (CHI 660E, Chenhua Corp., Shanghai, China). The three-electrode system consisted of a working electrode, a platinum wire counter electrode, and a saturated calomel reference electrode (SCE, ~0.244 V *vs.* NHE). Unless otherwise noted, all potentials were reported *vs.* NHE without iR compensation. Prior to cyclic voltammetry experiments, a bare glassy carbon electrode (0.071 cm^2) of 3 mm diameter was wet polished with 0.05 μm Al_2O_3 powder to obtain a mirror surface, followed by sonication in distilled water for 10 s. Controlled potential electrolysis was conducted on a relatively large surface area glassy carbon plate (1.0 cm^2) pretreated by the same procedure. The solution was stirred during electrolysis. Quantitative chlorine analysis was conducted by standard iodometric titration techniques as reported in the literature.[13] Briefly, chlorine was swept by a nitrogen gas purge from a reaction flask containing **1-NP** ($c_{Ag^+} = 5.3$ μM) and 1 M NaCl in 0.1 M HNO_3 (12 mL) into an aqueous solution of sodium hydroxide (w_{NaOH} = 0.4%, 50 mL). After electrolysis, hydrochloric acid solution (8 M, 10 mL), aqueous starch solution (w = 0.2%, 5 mL) and potassium iodide (2.0 g) were added to an aqueous solution of sodium hydroxide. The reaction flask was left in the dark for 5 min. During the reaction, the aqueous starch solution gradually turned dark blue ($Cl_2 + 2I^- \rightarrow I_2 + 2Cl^-$). The dark blue starch/iodine solution was titrated by 0.01 M aqueous $Na_2S_2O_3$ solution ($2Na_2S_2O_3 + I_2 \rightarrow Na_2S_4O_6 + 2NaI$).

Acknowledgements

Financial support from NNSFC (21522206 and 21421064) and MOST (2013CB834501) is gratefully acknowledged. We are grateful to Profs. Mei-Xiang Wang and Ming-Tian Zhang (THU) for helpful discussions.

References

1 (*a*) *Modern Chlor-Alkali Technology*, ed. J. Moorhouse, Wiley-Blackwell, 2001, vol. 8; (*b*) S. Lakshmanan and T. Murugesan, *Clean Technol. Environ. Policy*, 2014, **16**, 225–234.
2 A. Steel, D. van Wijk, J.-P. Debelle, D. Clotman, C. Andersson, S. Gallet, M. Pauwels, S. Presow, F. Minne, D. Stevenson, C. Peeters and C. Peeters, *Chlorine Industry Review*, EuroChlor, 2011-2012.
3 (*a*) S. Trasatti, *Electrochim. Acta*, 1987, **32**, 369–382; (*b*) S. Trasatti, *Electrochim. Acta*, 2000, **45**, 2377–2385; (*c*) R. K. B. Karlsson and A. Cornell, *Chem. Rev.*, 2016, **116**, 2982–3028.
4 (*a*) K. S. Exner, J. Anton, T. Jacob and H. Over, *Angew. Chem., Int. Ed.*, 2014, **53**, 11032–11035; (*b*) K. S. Exner, J. Anton, T. Jacob and H. Over, *Angew. Chem., Int. Ed.*, 2016, **55**, 7501–7504.
5 *Electrochemical Methods*, ed. A. J. Bard and L. R. Faulkner, Wiley, New York, 1980.
6 H. Over, *Chem. Rev.*, 2012, **112**, 3356–3426.
7 P. Duby, *JOM*, 1993, **45**, 41–43.
8 A. R. Zeradjanin, T. Schilling, S. Seisel, M. Bron and W. Schuhamnn, *Anal. Chem.*, 2011, **83**, 7645–7650.
9 C. D. Ellis, J. A. Gilbert, W. R. Murphy and T. J. Meyer, *J. Am. Chem. Soc.*, 1983, **105**, 4842–4843.
10 S. Ferrere and B. A. Gregg, *J. Chem. Soc., Faraday Trans.*, 1998, **94**, 2827–2833.
11 K. Aoki, H. Chen and J. Chen, *Electrochem. Commun.*, 2007, **9**, 2304–2307.
12 *Silver in Organic Chemistry*, ed. M. Harmata, Wiley & Sons, Inc., 2010.
13 J. Du, Z. Chen, C. Chen and T. J. Meyer, *J. Am. Chem. Soc.*, 2015, **137**, 3193–3196.
14 C. An, S. Peng and Y. Sun, *Adv. Mater.*, 2010, **22**, 2570–2574.
15 R. P. Bagwe and K. C. Khilar, *Langmuir*, 1997, **13**, 6432–6438.
16 Z. Lou, B. Huang, P. Wang, Z. Wang, X. Qin, X. Zhang, H. Cheng, Z. Zheng and Y. Dai, *Dalton Trans.*, 2011, **40**, 4104–4110.
17 X. He, Y. Wang, C.-Y. Gao, H. Jiang and L. Zhao, *Chem. Sci.*, 2015, **6**, 654–658.
18 (*a*) C. Di Nicola, Effendy, F. Fazaroh, C. Pettinari, B. W. Skelton, N. Somers and A. H. White, *Inorg. Chim. Acta*, 2005, **358**, 720–734; (*b*) C. W. Liu, B.-J. Liaw, L.-S. Liou and J.-C. Wang, *Chem. Commun.*, 2005, 1983–1985.
19 (*a*) P. Pyykkö, *Chem. Rev.*, 1997, **97**, 597–636; (*b*) H. Schmidbaur and A. Schier, *Angew. Chem., Int. Ed.*, 2015, **54**, 746–784.
20 E.-X. Zhang, D.-X. Wang, Q.-Y. Zheng and M.-X. Wang, *Org. Lett.*, 2008, **10**, 2565–2568.
21 C.-Y. Gao, L. Zhao and M.-X. Wang, *J. Am. Chem. Soc.*, 2012, **134**, 824–827.
22 M. Hargittai, *Chem. Rev.*, 2000, **100**, 2233–2301.
23 (*a*) P. Wang, B. Huang, X. Qin, X. Zhang, Y. Dai, J. Wei and M.-H. Whangbo, *Angew. Chem., Int. Ed.*, 2008, **47**, 7931–7933; (*b*) Y. Tang, Z. Jiang, G. Xing, A. Li, P. D. Kanhere, Y. Zhang, T. C. Sum, S. Li, X. Chen, Z. Dong and Z. Chen, *Adv. Funct. Mater.*, 2013, **23**, 2932–2940.
24 (*a*) Q. Huang, S. Wen and X. Zhu, *RSC Adv.*, 2014, **4**, 37187–37192; (*b*) D. Amaranatha Reddy, J. Choi, S. Lee, R. Ma and T. K. Kim, *RSC Adv.*, 2015, **5**, 67394–67404.
25 Y. Sun and Y. Xia, *J. Am. Chem. Soc.*, 2004, **126**, 3892–3901.
26 J. F. Moulder, W. F. Stickle, P. E. Sobol and K. D. Bomben, in *Handbook of X-ray Photoelectron Spectroscopy*, ed. J. Chastain and R. C. King, Physical Electronics, Minnesota, 1992.
27 T. X. Wang and D. W. Margerum, *Inorg. Chem.*, 1994, **33**, 1050–1055.
28 G. M. Sheldrick, *Acta Crystallogr., Sect. A: Found. Crystallogr.*, 2008, **64**, 112–122.

